Article:
Kim, Sanghoon, De bruyn, Mario, Alauzun, Johan G. et al. (2018) Alginic acid-derived mesoporous carbonaceous materials (Starbon®) as negative electrodes for lithium ion batteries: Importance of porosity and electronic conductivity. Journal of Power Sources. pp. 18-25. ISSN: 0378-7753

https://doi.org/10.1016/j.jpowsour.2018.10.026

Alginic acid-derived mesoporous carbonaceous materials (Starbon®) as negative electrodes for lithium ion batteries: importance of porosity and electronic conductivity

Sanghoon Kim,[*,a] Mario De bruyn,[b,c] Johan G. Alauzun,[a] Nicolas Louvain,[a,d] Nicolas Brun,[a] Duncan J. Macquarrie,[b] Lorenzo Stievano,[a,d] Bruno Boury,[a] P. Hubert Mutin[a] and Laure Monconduit,[*,a,d]

a. Institut Charles Gerhardt Montpellier, Université de Montpellier, CNRS, Montpellier, France.

b. Green Chemistry Centre of Excellence, University of York, York, North Yorkshire, YO10 5DD, UK.

c. Faculty of Science, Debye Institute for Nanomaterials Science, Utrecht University, Universiteitsweg 99, CG Utrecht 3584, The Netherlands.

d. Réseau sur le Stockage Electrochimique de l'Energie (RS2E), CNRS FR3459, 33 Rue Saint Leu, 80039 Amiens Cedex, France.

*Corresponding authors. Tel : +33 (0)4 67 14 90 99, E-mail : sanghoon.kim@umontpellier.fr (Sanghoon Kim) / Tel: +33 (0)4 67 14 33 35, E-mail: laure.monconduit@umontpellier.fr (Laure Monconduit)

Graphical Abstract

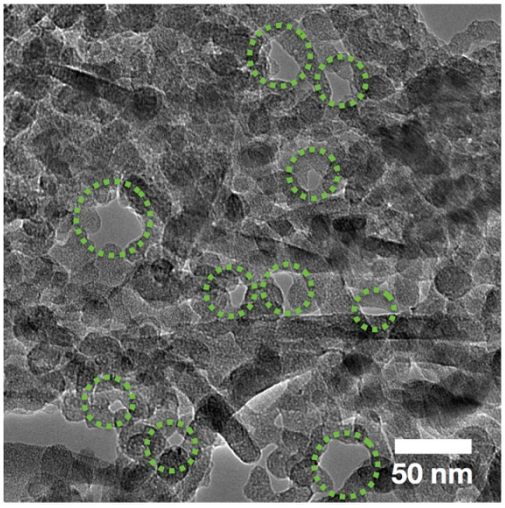

Alginic acid-derived mesoporous carbonaceous material (Starbon® A800)

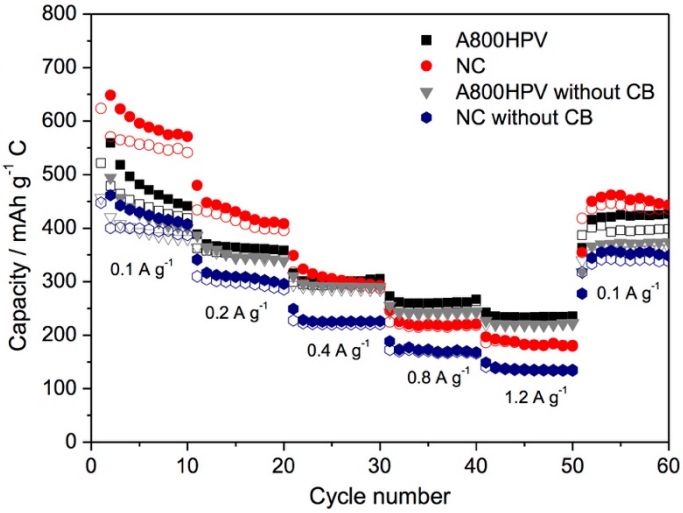

Excellent electrochemical performance as negative electrode lithium ion batteries

Abstract

Alginic acid-derived mesoporous carbonaceous materials (Starbon® A800 series) were investigated as negative electrodes for lithium ion batteries. To this extent, a set of mesoporous carbons with different pore volume and electronic conductivity was tested. The best electrochemical performance was obtained for A800 with High Pore Volume (A800HPV), which displays both the highest pore volume (0.9 cm^3 g^{-1}) and the highest electronic conductivity (84 S m^{-1}) of the tested materials. When compared to a commercial mesoporous carbon, A800HPV was found to exhibit both a better long-term stability, and a markedly improved rate capability. The presence of a hierarchical interconnected pore network in A800HPV, accounting for a high electrolyte accessibility, could lay at the origin of the good electrochemical performance. Overall, the electronic conductivity and the mesopore size appear to be the most important parameters, much more than the specific surface area. Finally, A800HPV electrodes display similar electrochemical performance when formulated with or without added conductive additive, which could make for a simpler and more eco-friendly electrode processing.

1. Introduction

For more than 20 years, lithium ion batteries (LIB) have been the most important power sources for a variety of applications such as portable electronic devices and electric vehicles. This is mainly due to their high energy density, long life cycle and low toxicity compared to conventional (rechargeable) batteries such as lead-acid, Ni-Cd, or NiMH.[1,2] To date, graphite is still the most used negative electrode material in commercially available LIB. This relates mainly to its low cost and low working potential of the Li-intercalation process.[3,4] However, because of its limited rate capability and the occurrence of unwanted side reactions, such as the growth of Li-dendrites on the anode surface,[5] the use of graphite as a negative electrode material in large scale battery systems (*e.g.*, for electric vehicles) is still challenging.[6,7] In addition, with the advent of next generation cathode materials such as sulfur [8], an important mismatch in capacity between the cathode and the anode might arise. Indeed, sulfur cathodes are expected to yield specific capacities close to the theoretical one, *i.e.*, 1675 mAh g^{-1}, versus only 372 mAh g^{-1} for graphite. Accordingly, the development of negative electrode materials with a high specific capacity is needed.

As alternative materials to graphite, a variety of nano-structured carbonaceous materials have been proposed, such as carbon nanotubes,[9,10] graphene,[11,12] hollow carbon spheres,[13,14] porous carbons [15-18] or hybrids between all these systems [19,20]. Doping by heteroatoms such as nitrogen [21,22] or boron[23] has also been investigated. Mesoporous carbons and more particularly carbons with a hierarchical pore structure were found of particular interest as interconnected pores can provide an efficient Li-ion pathway, while a high specific surface area could improve the charge-transfer processes at the electrode-electrolyte interface.[15] As a result, mesoporous carbon-based negative materials could combine high rate capability with a long term cyclability.

Environmental issues being of increasing concern, the use of benign and sustainable materials constitutes an appreciable asset. Starbon® carbonaceous materials are typically derived from polysaccharides and most notably alginic acid and starch. Depending on the nature of the starting polysaccharides, the processing method (e.g. supercritical drying or freeze drying, solvent exchange or *tert*-butanol addition), and the thermal transformation step (temperature, heating rate), these carbonaceous materials can be produced with a wide range of surface chemistries and textures.[24-27] To date, Starbon® materials have been applied successfully to several catalytic reactions,[28-30] (in)organic adsorption processes,[31-34] and as a stationary phase for liquid chromatography.[25] Additionally they were also used as porous templates for the design of heterogeneous catalysts (Pd, TiO_2).[35,36] Very recently we showed that Starbon® can also been used as an alternative carbon additive for $Li_4Ti_5O_{12}$ and TiO_2 electrodes, leading to significant improvements in battery performance.[37] This was ascribed to efficient Li-ion diffusion in the mesoporous network combined with a relatively good electronic conductivity (84 S m^{-1}).

Here, the use of Starbon® A800 (alginic acid derived Starbon, carbonized at 800 °C) as an anode for LIB without the need of any conductive carbon additive is demonstrated. More specifically, the electrochemical performance of A800 is very similar to that of a commercially available mesoporous carbon (NC® series from EnerG2). This unexpected behavior is ascribed to the high mesopore volume and high conductivity of A800.

2. Experimental Section

2.1. Materials

Alginic acid from brown algae was purchased from Sigma-Aldrich (France). *Tert*-butyl alcohol (> 99 %) was obtained from Fluka (UK). Super P (> 99 %) was purchased from Alfa Aesar

(France). A commercial mesoporous carbon (NC series carbon, reference: PT NC-23) was obtained from EnerG2 (USA).[38] All reagents were used without further purification.

2.2 Synthesis of alginic acid-derived mesoporous carbonaceous materials (Starbon® A800)

Alginic acid-derived mesoporous carbonaceous materials were prepared via a direct carbonization of a dried expanded gel of alginic acid as described previously.[27] Briefly, an alginic acid solution (4.8 wt% in water) was gelled by heating it at 90 °C for 2.5 h after which it was cooled then kept at 4 °C for 24 h. To the resulting gel, *tert*-butyl alcohol was added in order to reach a 30 wt% *tert*-butyl alcohol/water eutectic composition. The mixture was stirred for 1 h at room temperature, kept at 4 °C for another 24 h, and then freeze dried (-85 °C) yielding a dry expanded alginic acid cryogel. The latter was carbonized at 800 °C for 3 h under argon flow (50 mL min^{-1}) with a heating rate of 1, 5 or 10 °C min^{-1}, leading to A800HPV (High Pore Volume), A800MPV (Medium Pore Volume) A800LPV (Low Pore Volume), respectively.[37] The yield of the carbonized materials was ≈25%.

2.3 Characterization

XRD patterns were obtained using a PANalytical X'Pert Pro MPD diffractometer, with the Kα radiation of Cu (λ = 1.5418 Å) and a step size of 0.033 into the 10°–90° range. N_2 physisorption experiments were carried out at -196 °C on a Micromeritics 3Flex; all carbon samples were degassed at 120 °C for 15 h under high vacuum (ca. 0.1 Pa) before physisorption measurements. Scanning electron microscopy (SEM) images were acquired with a Hitachi S-4800 electron microscope Transmission electron microscopy (TEM) images were acquired using JEOL FX2200 microscope. Raman spectra were obtained on a Horiba Jobin-Yvon LabRAM ARAMIS micro- spectrometer with an excitation wavelength of 473 nm. The electronic

conductivity of carbon additives was measured by a 4-point probe method on pellet (30 mg carbon + 2 mg PTFE, 13 mm diameter) prepared using a FT-IR pellet press (5 tons).

Galvanostatic electrochemical characterizations were performed at RT on a BTS3000 instrument (Neware Battery). Cyclic voltammetry (CV) measurements were carried out on VSP-300 instrument with scan rate of 0.1 mV s^{-1} to 10 mV s^{-1}. Electrochemical impedance spectroscopy (EIS) studies were done on a BioLogic VSP-300 instrument, from 100 kHz to 20 mHz, with a 10 mV amplitude. Electrode slurry with 2 different formulations was prepared using active materials (A800 series carbon or NC carbon), Super P (conductive carbon additive) and polyvinylidene fluoride (PVDF) (binder) in the mass ratio of 8:1:1 or 9:0:1. After stirring in N-methyl-2-pyrrolidone (NMP), the slurry was mixed using an agate grinding jar (1 h at 500 rpm), then tape casted uniformly at 150 μm onto a copper current collector (0.018 mm, > 99.96 %, Prometor) using a 3540 bird film applicator (Elcometer). Electrodes (diameter 12.7 mm) were cut with a disk cutter and dried under vacuum at 90 °C for 15 h. The loading weight was ca. 1.5 mg / per electrode disk. CR2032 coin-type cells were assembled in a glove box (MBraun) under Ar atmosphere (O_2 < 0.5 ppm, H_2O < 0.5 ppm), using lithium metal as both reference and counter electrode. The electrolyte was LP30 (1M $LiPF_6$ dissolved in a mixture of ethylene carbonate (EC) and dimethyl carbonate (DMC) (ratio EC:DMC = 1:1). Whatman glass fibre disks were used as separators. The electrochemical galvanostatic measurements were taken in the voltage range of 3.00–0.01 V versus Li^+/Li at different current densities.

3. Results and discussion

3.1 Synthesis and characterization of A800 samples and the comparison with NC carbon

First, several carbonization temperatures of the dried expanded gel of alginic acid were investigated: carbonization at lower temperatures like 300 °C yields poorly carbonized product, for example, A300 (carbonized at 300 °C) shows C:O atomic ratio of only 4.4. When the dried

expanded gel of alginic acid was carbonized at higher temperature, a continuous decrease of pore volume and pore size was observed, while the carbonization degree remained almost the same. (more details in Table S1) As a result, a carbonization temperature of 800 °C was found to be optimal, thus chosen in this study.

The structural features of the different carbons (A800 series, NC carbon) was investigated by XRD and Raman spectroscopy. XRD patterns (Fig. 1a) display two peaks at 22.1 ° and 43.9 ° which can be assigned to the 002 and 100 planes of graphitic carbon. However, compared to the XRD pattern of graphite,[5] these peaks are much less intense suggesting that both the A800 materials and NC carbon are largely amorphous.

Table 1. Heating rate in the carbonization step, textural properties, electronic conductivity and C:O ratio of carbon materials used in this study[a]

Sample	Heating rate (°C min^{-1})	S_{BET} (m^2 g^{-1})	PV_{total} (cm^3 g^{-1})	PV_{meso} (cm^3 g^{-1})	D_p (nm)	σ (S m^{-1})	C:O ratio	Discharge / charge capacity at 1st cycle (mAh g^{-1})	Coulombic efficiency at 1st cycle
A800HPV	1	490	0.91	0.71	16.0	84	16.9	1176 / 504	43 %
A800MPV	5	570	0.59	0.43	12.5	37	17.8	723 / 319	44 %
A800LPV	10	370	0.34	0.20	10.2	23	17.2	489 / 210	43 %
NC	NA	1370	1.33	0.89	6.2	32	19.6	1634 / 622	38 %

[a.] S_{BET}: BET specific surface area; PV_{total}: total pore volume at P/P_0 = 0.99; PV_{meso}: BJH mesopore volume between 2 and 50 nm; D_p: BJH average mesopore diameter calculated from the desorption branch; σ: electronic conductivity; C:O atomic ratio obtained by SEM-EDX.

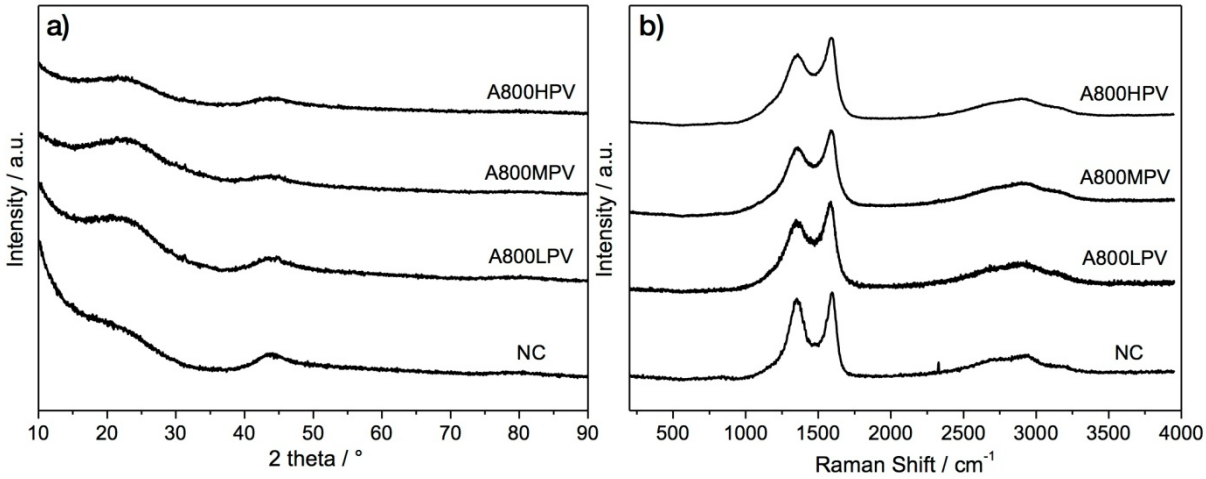

Fig. 1. a) XRD patterns and b) Raman spectra of carbon materials investigated in this study

Fig. 1b displays the recorded Raman spectra. D and G bands can be seen at 1345 cm^{-1} and 1583 cm^{-1}, respectively. In addition, two to three broad peaks are observed in the 2650 to 3150 cm^{-1} region. These peaks relate likely to the 2D (2690 cm^{-1}) and D + G bands (2960 cm^{-1}) of carbonaceous materials [39] and are typical of a disordered pseudo-graphitic structure. For all A800 materials the I_D/I_G ratio was 0.81, suggesting that A800 materials are characterized by similar levels of graphitization, whereas a higher ratio (0.90) was obtained for NC carbon, showing that NC carbon was somewhat more graphitized than the A800 carbons series.

N_2 physisorption isotherms (Fig. 2) of all carbon materials were of type IV, indicating the presence of a mesoporous structure. The pore volume and the pore size (Table 1) decreased with increasing heating rate in the carbonization step. Horwath-Kawazoe analysis of the isotherms of A800HPV and NC carbon samples showed the presence of micropores, with micropore volumes of 0.20 and 0.44 $cm^3\ g^{-1}$, respectively. The micropore size distribution for A800HPV and NC carbon were very similar, with an average micropore size of around 0.5 nm (Fig. S1). A800HPV is highly mesoporous, as only ca. 20 % of pore volume is attributed to micropores, compared to ca. 35 % for NC carbon.

Although all tested A800 materials show a low level of graphitization, it is interesting to see that the electronic conductivity (σ) of A800 samples (Table 1) is decreased with increasing heating rate, probably because a lower heating rate allows more time for the carbonization/graphitization or a better connection among the graphitic domains.

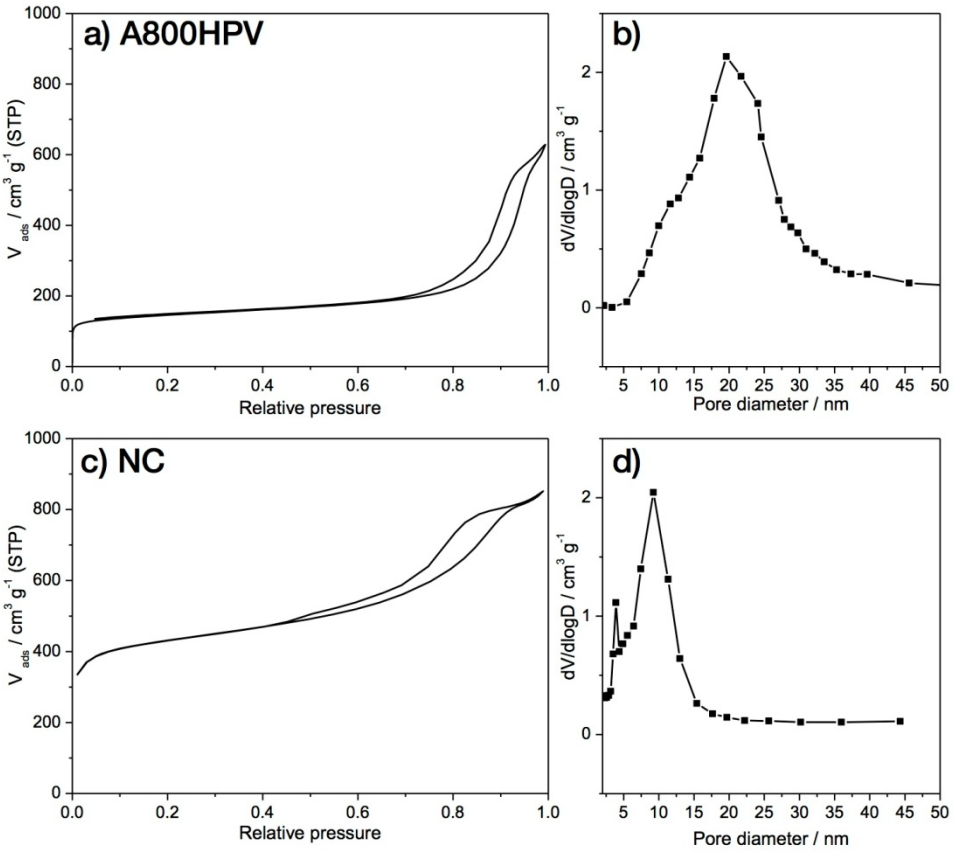

Fig. 2. N_2 physisorption isotherms and BJH pore size distribution of A800HPV and NC carbon. For A800MPV and A800LPV, see Fig. S2 (ESI).

The morphology of A800HPV and NC carbon was analyzed by SEM. As can be seen in Fig. 3a, A800HPV consists of large aggregates, up to 20 μm in size, resulting from the entanglement of the alginic acid chains in the gel state.[25] At higher magnification (Fig. 3b), large mesopores and macropores can be clearly observed. TEM measurements (Fig. 4a, b) confirmed the highly mesoporous nature of A800HPV and its hierarchical pore structure. In the case of NC carbon, the size of the aggregates is markedly smaller than the ones of A800HPV. At higher

magnification, its surface was found smoother than that of A800HPV and no large mesopores or macropores could be observed. TEM images also confirmed that the mesopores are significantly smaller than that of A800HPV, in agreement with N_2 physisorption results.

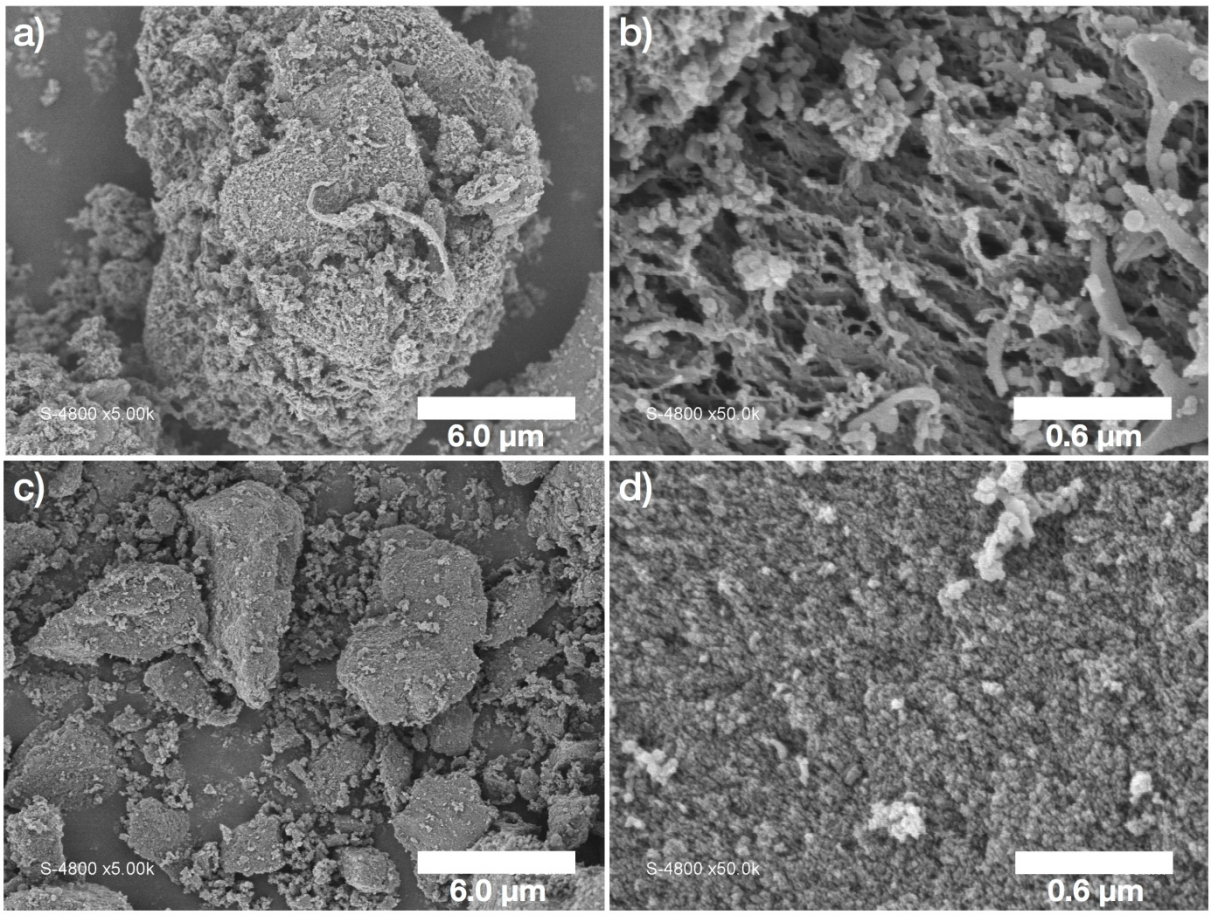

Fig. 3. SEM images of A800HPV (a and b) and NC carbon (c and d).

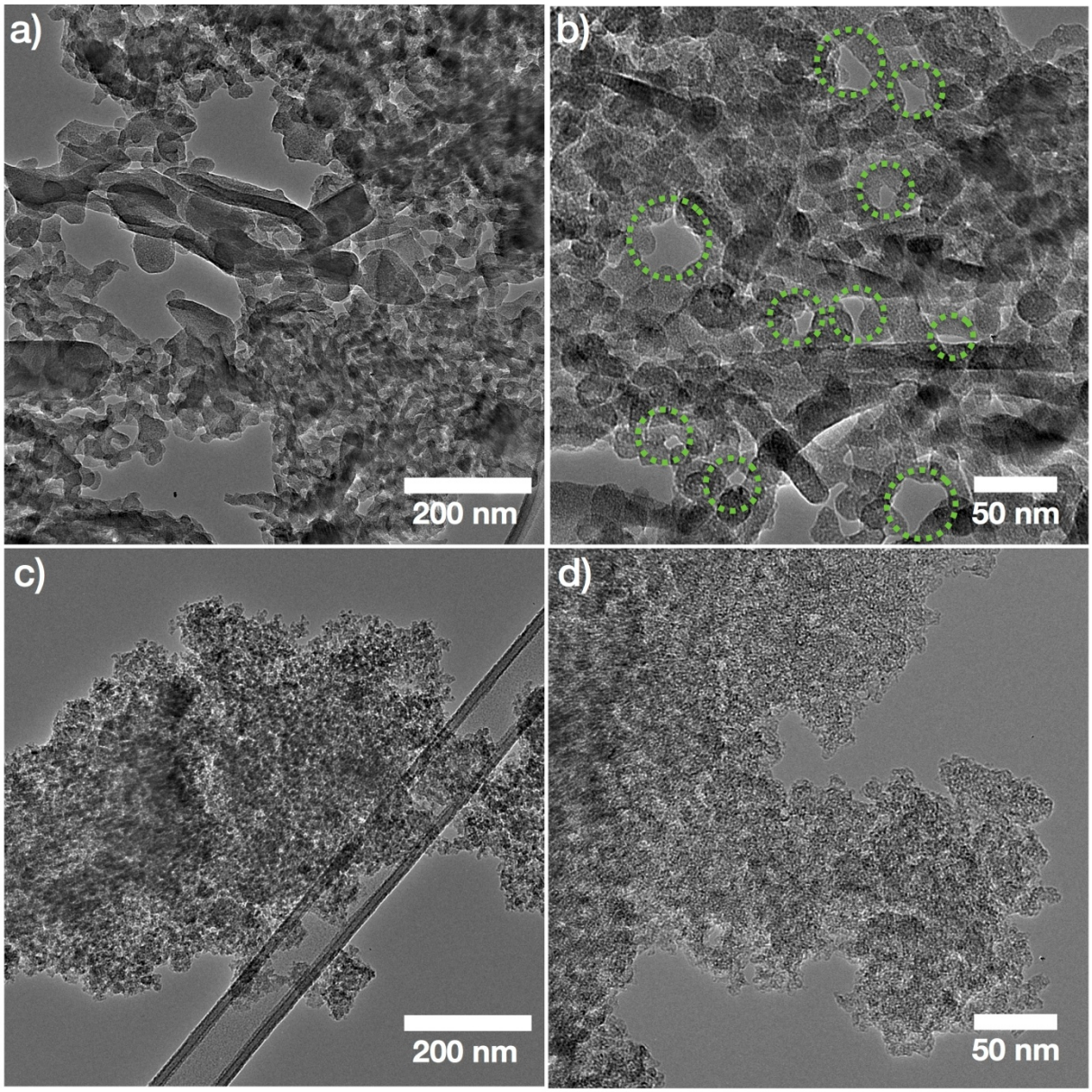

Fig. 4. TEM image of A800HPV (a and b) and NC carbon (c and d). Meso and macropores in A800HPV highlighted by yellow circles.

3.2 Electrochemical performance of A800 samples and the comparison with NC carbon

The different A800 samples and the commercial mesoporous carbon were evaluated as negative materials for LIB.

Firstly, the electrochemical performance of the A800 samples was investigated by galvanostatic discharge-charge measurement at different current densities. As shown in Fig. 5a, the

A800HPV electrode shows the best performance among A800 samples, showing ≈50% higher discharge capacity compared to A800MPV (420 mAh g^{-1} for A800HPV vs 280 mAh g^{-1} for A800MPV, 10^{th} cycle at 0.1 A g^{-1}). This behavior has to be ascribed mainly to the high mesopore volume and large pore size of A800HPV as well as its high electronic conductivity. Therefore, A800HPV was further characterized and compared to a commercial mesoporous carbon (NC carbon).

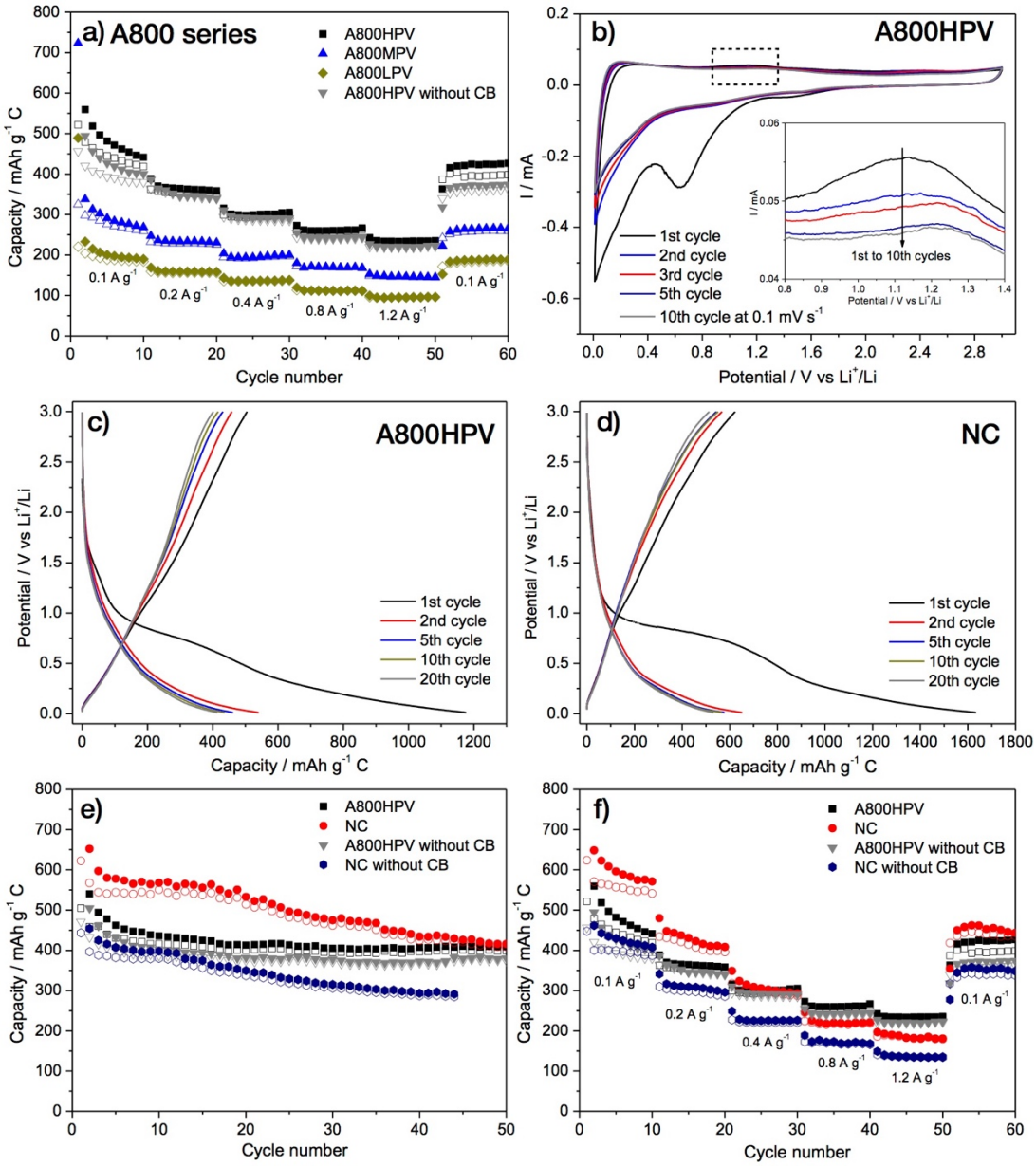

Fig. 5. Electrochemical properties of carbon materials a) Rate capability test for A800 series electrodes (filled and open symbols refer to discharge and charge, respectively), b) CV curve

of A800HPV electrode at the scan rate of 0.1 mV s^{-1} and zoomed image of selected zone (inset), c) Galvanostatic discharge-charge profile for A800HPV electrode vs Li, d) Galvanostatic discharge-charge profile for NC carbon electrode vs Li, e) Cycling test for A800HPV electrode and NC carbon electrode with/without conductive carbon additive (CB) at current density of 0.1 A g^{-1}, f) Rate capability test for A800HPV electrodes and NC carbon electrodes with/without conductive carbon additive (CB).

Cyclic voltammetry at a scan rate of 0.1 mV s^{-1} within the 0.01 to 3.0 V (vs Li^+/Li) voltage range was performed on A800HPV. As shown in Fig. 5b, two cathodic peaks at 1.4 V and 0.7 V are observed only for the first scan, and can be assigned to some irreversible reactions such as the reaction of Li^+ with oxygenated surface groups [13] in A800HPV (1.4 V) and the decomposition of electrolyte (0.7 V), resulting in the formation of solid electrolyte interphase (SEI). These peaks disappear from the second cycle onwards leaving only a peak at ≈0.1 V ascribed to the reversible insertion of lithium into the carbon structure. During the reverse reaction (0.01 to 3.00 V vs Li^+/Li), a broad and small peak corresponding to the extraction of Li from the carbon is observed ~0.15 V. In addition, a shoulder-like peak around 1.2 V can be attributed to the partial decomposition of SEI, which was formed during the cathodic scan.[40] From the second cycle onwards, the CV profiles are almost identical. Noteworthy is the continued decrease of the peak at 1.2 V corresponding to the partial decomposition of the SEI,[17] especially for 5^{th} and 10^{th} cycle (Fig. 5a, inset). This result indicates that both the structure of the A800HPV electrode and the SEI are particularly stable. This was further confirmed by galvanostatic discharge-charge experiments as presented below.

Fig. 5c shows a representative galvanostatic discharge-charge profile of the A800HPV electrode when tested at a current density of 0.1 A g^{-1} within a voltage range of 0.01–3.00 V vs. Li^+/Li for 20 cycles. The specific discharge capacity of A800HPV in the first cycle (1191 mAh g^{-1}) is markedly higher than in the subsequent cycles. This is mainly attributed to the

decomposition of the electrolyte and the formation of the SEI layer, which can be observed as a pseudo-plateau around 0.7 V. The specific discharge capacity for the second cycle is 571 mAh g^{-1}. This value further decreases in subsequent cycles until the 10^{th} cycle after which it stabilizes at ≈420 mAh g^{-1} until the final 50^{th} cycle. By comparison the commercial mesoporous NC carbon (Fig. 5d), which has a 3 times higher surface area than that of A800HPV, the pseudo-plateau linked to the formation of the SEI layer appears around 0.9 V and its shape is more pronounced. This suggests that the electrolyte decomposition is enhanced with A800HPV, which is likely due to its high specific surface area. This pseudo-plateau corresponds to a capacity around 700 $mAhg^{-1}$ very similar for both the NC and A800HPV electrodes. This suggests that the Li insertion mechanisms is similar in A800HPV and NC carbon, in spite of their different surface area. It is noteworthy here that the capacity calculated from galvanostatic discharge-charge profiles of carbon always includes the contribution of the decomposition of the electrolyte (or in other words the contribution due to the formation of the SEI layer), which cannot be neglected. In addition, with high specific surface carbon materials cycled at a relatively low current density (here a 0.1 A g^{-1}), the decomposition of the electrolyte is enhanced by the long the time spent at low voltage.[41] For subsequent cycles, the discharge capacity of NC decreases monotonically from 674 mAh g^{-1} (2nd cycle) to 520 mAh g^{-1} (20^{th} cycle). It is however noteworthy that in contrast to the A800HPV electrode, the discharge capacity of NC carbon does not stabilize, not even over 50 consecutive cycles (Fig. 5e), and the specific discharge capacities after 50 cycles of NC and A800HPV are identical. The higher discharge capacity of NC in the first few cycles is probably due to a continuous decomposition of the electrolyte at the lower voltages on the high surface area. This result is not fully consistent with previously reported works, where invariably a high specific surface area is the predominant factor for porous carbon negative materials in LIB.[14,18,22] However, as shown with the

different A800 samples, the pore volume (or pore size) might also influence the electrochemical performance.

Another advantage of A800HPV over NC lays in its electronic conductivity, which has been determined at 84 S m^{-1} for A800HPV, whereas the conductivity of NC is limited to 32 S m^{-1}. To understand fully the role of the electronic conductivity, an electrode without conductive carbon additive (CB) was formulated for both A800HPV and NC. As shown in Fig. 5e, the specific discharge capacity gap between the A800HPV electrode with and without CB is only ca. 20-30 mAh g^{-1}. In the case of NC carbon, this gap is with 150 mAh g^{-1} appreciably more significant. If one also subtracts the capacity contribution from the conductive carbon additive (depending on cycle number and electrolyte composition, Super P shows a specific capacity of ca. 150-200 mAh g^{-1},[41] and thus its contribution can be estimated to be 15-20 mAh g^{-1} as 10 wt% of Super P is added), the specific discharge capacity of A800HPV without CB is actually almost the same of that of A800HPV with CB. Furthermore, it is very interesting to see that the "A800HPV without CB" electrode actually exhibits a better coulombic efficiency (C.E.) (> 98.5 % after 30 cycles, Fig. S3) compared to the "A800HPV with CB" electrode (97.5 > C.E. > 96.5 % after 30 cycles). This indicates that some of the irreversibility observed with the "A800HPV with CB" electrode arises from the CB additive. Given the above stated findings, the good stability of A800HPV (including "A800HPV without CB" electrode) during cycling likely relates to its good electronic conductivity. Therefore, even though the presence of a highly conductive carbon additive (279 S m^{-1} for Super P) in an electrode can indeed help with the overall electrochemical performance for non-conductive carbon negative electrode materials (cf. NC vs NC without CB in Fig. 5e), the role of the CB additive seems here very limited, especially concerning the electrochemical stability of such carbon materials over cycling.

When considering the rate capability test (Fig. 5f), the "A800HPV with CB" and "A800HPV without CB" electrodes show a slightly higher specific capacity than their respective NC carbon counterparts at 0.8 A g^{-1} and 1.2 A g^{-1}. This is attributed to the high electronic conductivity of A800HPV and may also relate to the large pore size. Such link between pore diameter and Li-ion diffusivity was shown before by Li et al [40]. In agreement with this paper, we have observed that the influence of the pore size is actually more pronounced when high current densities are applied. The importance of the pore size at high current densities was further investigated by comparing NC with A800MPV. A800MPV shows a very similar electron conductivity (37 S m^{-1}) as NC (32 S m^{-1}), while its average mesopore size is with 13 nm still twice higher than that of NC. As shown in Fig. 5a, the specific discharge capacity of A800MPV at 1.2 A g^{-1} is 165 mAh g^{-1}, which is only 25 mAh g^{-1} less than the specific discharge capacity of NC at the same current density. In this respect, it is worth mentioning that the surface areas of A800MPV and NC differ by a factor of two (570 m^2 g^{-1} for A800MPV vs 1370 m^2 g^{-1} for NC). One can thus conclude that for porous carbon negative electrodes, the electronic conductivity, the mesopore size and the hierarchical porosity are very important parameters and more so than simply the surface area. When comparing the electrochemical performance of A800HPV with graphite, which has already been widely used in LIB, A800HPV with/without CB electrode shows a better performance both at low and high current densities (*e.g.* 380 mAh g^{-1} for 'A800HPV with CB' at 0.2 A g^{-1} compared to 320 mAh g^{-1} for graphite at 0.186 A g^{-1}, 10^{th} cycle See Fig. S4). Model carbons elaborated by the hard templating method can reach higher capacities, for example, a cubic structured ordered mesoporous carbon CMK-8 shows ca. 600 mAh g^{-1} at 0.1 A g^{-1}, while 440 mAh g^{-1} at 0.1 A g^{-1} was obtained A800HPV electrode.[17] However, Starbon® A800HPV can be easily synthesized from alginic acid without any template, which represents an obvious advantage over hard templated carbons, in term of large scale synthesis and cost. In addition, it should be noted that the electrochemical

performance of carbon highly depends on electrode composition, cycling voltage range, electrolyte and cell fabrication, thus a precise comparison is difficult.[41]

Given the interesting results with the "A800HPV without CB" electrode, electrochemical impedance spectroscopy (ESI) analysis was carried out on the A800HPV with and without CB electrodes. As shown in Fig. 6, the Nyquist plots for fresh electrochemical cells using the A800HPV with/without CB electrodes, exhibit a single semicircle at the high-to-middle frequency range. From these the charge transfer resistance (R_{ct}) values can be calculated. With respective values of 59 Ω and 54 Ω for the "A800HPV without CB" and "A800HPV with CB" electrodes these R_{ct} are very similar. With cycling the R_{ct} values decrease to 41 and 36 Ω without and with CB, respectively, after the 20th cycle. This result shows once again that A800HPV can provide by itself the electronic conductivity needed for a good electrochemical performance.

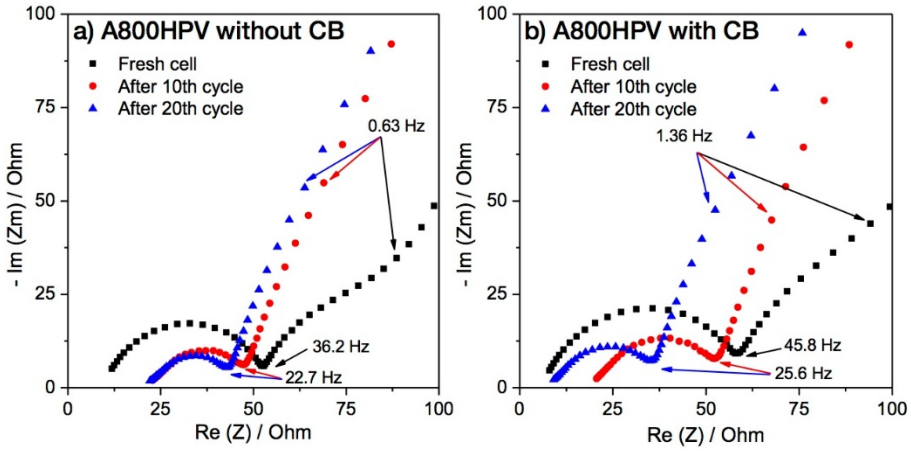

Fig. 6. The Nyquist plots for a) 'A800HPV without CB' electrode and b) 'A800HPV with CB' electrode, obtained at charge state.

Finally, to better understand the charge storage mechanism in the A800HPV electrode, cyclic voltammetry at different scan rates (0.1 mV s^{-1} to 10 mV s^{-1}) was performed (Fig. 7a for only 'A800HPV with CB' electrode). Briefly, the total capacity can usually be divided into the Faradaic contribution (notably the formation of SEI and Li^+ intercalation) and the non-faradaic

contribution (e.g.(pseudo)-capacitive charge storage). In order to calculate each contribution, cyclic voltammetry curves at different scan rates were analyzed following equation (1) :[42]

$$i(v) = av^b \quad (1)$$

Plotting the scan rate v versus the measured current i, the b-values can be determined. In the case of a Faradaic contribution, b-values are generally close to 0.5, whereas a dominance of the non-faradaic contribution would yield b-values approach 1.[43,44] As can be inferred from Fig. 7b the "A800HPV with CB" electrode display b-values between 0.7 and 0.84 which points at both faradaic and non-faradaic contributions while the faradaic contribution slightly increased at low voltages like 0.2 V, 0.4 V (b-value of 0.70 for 0.2 V), where Li insertion process mainly occurs. In the case of the "A800HPV without CB" electrode the retrieved b-values vary between 0.75 and 0.85, somewhat higher than those for the "A800HPV with CB" electrode, and this especially at 0.2 V. This implies that for the "A800HPV without CB" electrode, the faradaic contribution at low voltages is somewhat lower than for the "A800HPV with CB" electrode. This could be explained by assuming that at low voltages the SEI layer formation (which is a Faradaic response) relates mainly to the presence of the conductive carbon additive. This can in principle also be derived from the galvanostatic discharge-charge profile (Fig. 5d) showing a lower coulombic efficiency for the "A800HPV with CB" electrode, compared to the "A800HPV without CB" electrode.

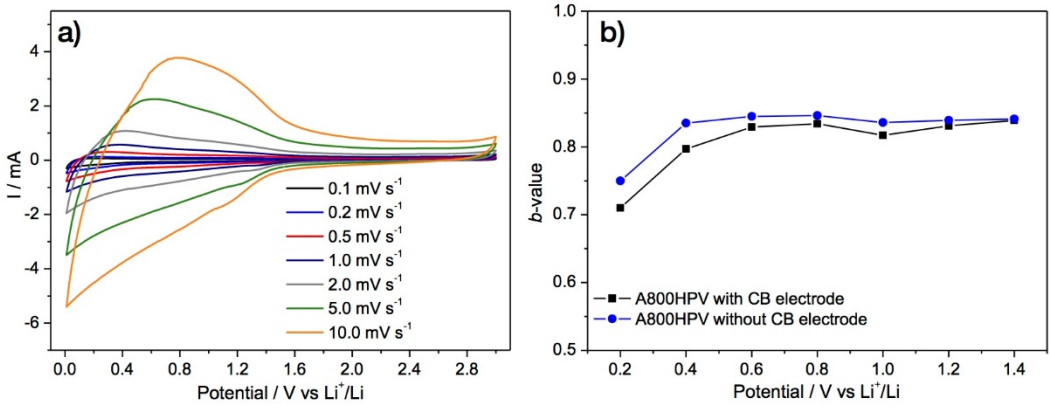

Fig. 7. a) CV curves of A800HPV (with CB) electrode at various scan rates (2nd cycle), from 0.1 mV s^{-1} to 10.0 mV s^{-1}, b) calculated b-values for A800HPV with/without CB electrode as a function of the cathodic (lithium insertion) sweep.

4. Conclusion

In conclusion, alginic acid-derived mesoporous carbon materials (A800 samples) were investigated as negative electrode for lithium ion batteries. These samples have similar specific surface area but different pore volumes. The specific capacity of these materials increases with the pore volume, showing the importance of the presence of large pores to facilitate Li-ion diffusion. Comparison of the best A800 sample (A800HPV with the highest pore volume) to a commercial mesoporous carbon (NC carbon) with a very high specific surface area and pore volume confirms the importance of a hierarchical pore structure with large mesopores and macropores. Finally, owing to its higher electronic conductivity, A800HPV electrodes can be formulated without carbon black without impacting the electrochemical performance, contrary to NC carbon.

Our results suggest that polysaccharide-derived mesoporous carbons could be used to design eco-friendlier electrodes for LIB.

Acknowledgements

Financial support was received by the European Commission in the framework of POROUS4APP project (H2020 GA no. 666157). The authors would like to thank Didier Cot (IEM, France) for SEM analysis. Lea Daenens (ICGM, France) is gratefully acknowledged for technical help in the collection of the Raman spectra.

References

[1] M. Armand, J.M. Tarascon, Building better batteries, Nature. 451 (2008) 652–657.

[2] V. Etacheri, R. Marom, R. Elazari, G. Salitra, D. Aurbach, Challenges in the development of advanced Li-ion batteries: a review, Energy Environ. Sci. 4 (2011) 3243–3262.

[3] J.R. Dahn, T. Zheng, Y. Liu, J.S. Xue, Mechanisms for Lithium Insertion in Carbonaceous Materials, Science. 270 (1995) 590–593.

[4] S. Flandrois, B. Simon, Carbon materials for lithium-ion rechargeable batteries, Carbon. 37 (1999) 165–180.

[5] Z. Guo, J. Zhu, J. Feng, S. Du, Direct in situ observation and explanation of lithium dendrite of commercial graphite electrodes, RSC Adv. 5 (2015) 69514–69521.

[6] B. Scrosati, J. Hassoun, Y.-K. Sun, Lithium-ion batteries. A look into the future, Energy Environ. Sci. 4 (2011) 3287–9.

[7] M.M. Thackeray, C. Wolverton, E.D. Isaacs, Electrical energy storage for transportation—approaching the limits of, and going beyond, lithium-ion batteries, Energy Environ. Sci. 5 (2012) 7854–7863.

[8] Y. Yang, G. Zheng, Y. Cui, Nanostructured sulfur cathodes, Chem. Soc. Rev. 42 (2013) 3018–3032.

[9] B.J. Landi, M.J. Ganter, C.D. Cress, R.A. DiLeo, R.P. Raffaelle, Carbon nanotubes for lithium ion batteries, Energy Environ. Sci. 2 (2009) 638–654.

[10] S. Yoon, S. Lee, S. Kim, K.-W. Park, D. Cho, Y. Jeong, Carbon nanotube film anodes for flexible lithium ion batteries, J. Power Sources. 279 (2015) 495–501.

[11] P. Guo, H. Song, X. Chen, Electrochemical performance of graphene nanosheets as anode material for lithium-ion batteries, Electrochem. Commun. 11 (2009) 1320–1324.

[12] J. Hassoun, F. Bonaccorso, M. Agostini, M. Angelucci, M.G. Betti, R. Cingolani, et al., An Advanced Lithium-Ion Battery Based on a Graphene Anode and a Lithium Iron

Phosphate Cathode, Nano Lett. 14 (2014) 4901–4906.

[13] K. Tang, R.J. White, X. Mu, M.-M. Titirici, P.A. van Aken, J. Maier, Hollow Carbon Nanospheres with a High Rate Capability for Lithium-Based Batteries, ChemSusChem. 5 (2012) 400–403.

[14] X. Yue, W. Sun, J. Zhang, F. Wang, Y. Yang, C. Lu, et al., Macro-mesoporous hollow carbon spheres as anodes for lithium-ion batteries with high rate capability and excellent cycling performance, J. Power Sources. 331 (2016) 10–15.

[15] A.D. Roberts, X. Li, H. Zhang, Porous carbon spheres and monoliths: morphology control, pore size tuning and their applications as Li-ion battery anode materials, Chem. Soc. Rev. 43 (2014) 4341–4356.

[16] X.-L. Wu, L.-L. Chen, S. Xin, Y.-X. Yin, Y.-G. Guo, Q.-S. Kong, et al., Preparation and Li Storage Properties of Hierarchical Porous Carbon Fibers Derived from Alginic Acid, ChemSusChem. 3 (2010) 703–707.

[17] D. Saikia, T.-H. Wang, C.-J. Chou, J. Fang, L.-D. Tsai, H.-M. Kao, A comparative study of ordered mesoporous carbons with different pore structures as anode materials for lithium-ion batteries, RSC Adv. 5 (2015) 42922–42930.

[18] B. Campbell, R. Ionescu, Z. Favors, C.S. Ozkan, M. Ozkan, Bio-Derived, Binderless, Hierarchically Porous Carbon Anodes for Li-ion Batteries, Sci. Rep. 5 (2015) 14575.

[19] W. Wang, I. Ruiz, S. Guo, Z. Favors, H.H. Bay, M. Ozkan, et al., Hybrid carbon nanotube and graphene nanostructures for lithium ion battery anodes, Nano Energy. 3 (2014) 113–118.

[20] B. Jin, F. Gao, Y.-F. Zhu, X.-Y. Lang, G.-F. Han, W. Gao, et al., Facile Synthesis of Non- Graphitizable Polypyrrole-Derived Carbon/Carbon Nanotubes for Lithium-ion Batteries, Sci. Rep. 6 (2015) 19317.

[21] T. Chen, L. Pan, T.A.J. Loh, D.H.C. Chua, Y. Yao, Q. Chen, D. Li, et al., Porous

nitrogen-doped carbon microspheres as anode materials for lithium ion batteries, Dalton Trans. 43 (2014) 14931–14935.

[22] Y. Cui, H. Wang, X. Xu, Y. Lv, J. Shi, W. Liu, et al., Nitrogen-doped porous carbons derived from a natural polysaccharide for multiple energy storage devices, Sustainable Energy Fuels. 2 (2018) 381–391.

[23] J.G. Kim, F. Liu, C.-W. Lee, Y.-S. Lee, J.S. Im, Boron-doped carbon prepared from PFO as a lithium-ion battery anode, Solid State Sci. 34 (2014) 38–42.

[24] V. Budarin, J.H. Clark, J.J.E. Hardy, R. Luque, K. Milkowski, S.J. Tavener, et al., Starbons: New Starch-Derived Mesoporous Carbonaceous Materials with Tunable Properties, Angew. Chem. Int. Ed. 45 (2006) 3782–3786.

[25] R.J. White, C. Antonio, V.L. Budarin, E. Bergström, J. Thomas-Oates, J.H. Clark, Polysaccharide-Derived Carbons for Polar Analyte Separations, Adv. Funct. Mater. 20 (2010) 1834–1841.

[26] R.J. White, V.L. Budarin, J.H. Clark, Pectin-Derived Porous Materials, Chem. Eur. J. 16 (2010) 1326–1335.

[27] A. Borisova, M. De Bruyn, V.L. Budarin, P.S. Shuttleworth, J.R. Dodson, M.L. Segatto, et al., A Sustainable Freeze-Drying Route to Porous Polysaccharides with Tailored Hierarchical Meso- and Macroporosity, Macromol. Rapid Commun. 36 (2015) 774–779.

[28] R. Luque, V. Budarin, J.H. Clark, D.J. Macquarrie, Microwave-assisted preparation of amides using a stable and reusable mesoporous carbonaceous solid acid, Green Chem. 11 (2009) 459–461.

[29] R. Luque, J.H. Clark, K. Yoshida, P.L. Gai, Efficient aqueous hydrogenation of biomass platform molecules using supported metal nanoparticles on Starbons®, Chem. Commun. (2009) 5305–5307.

[30] R. Luque, V. Budarin, J.H. Clark, D.J. Macquarrie, Glycerol transformations on polysaccharide derived mesoporous materials, Appl. Catal., B. 82 (2008) 157–162.

[31] A. Muñoz García, A.J. Hunt, V.L. Budarin, H.L. Parker, P.S. Shuttleworth, G.J. Ellis, et al., Starch-derived carbonaceous mesoporous materials (Starbon®) for the selective adsorption and recovery of critical metals, Green Chem. 17 (2015) 2146–2149.

[32] H.L. Parker, A.J. Hunt, V.L. Budarin, P.S. Shuttleworth, K.L. Miller, J.H. Clark, The importance of being porous: polysaccharide-derived mesoporous materials for use in dye adsorption, RSC Adv. 2 (2012) 8992–8997.

[33] J.R Dodson, H.L. Parker, A. Muñoz García, A. Hicken, K. Asemave, T.J. Farmer, et al., Bio-derived materials as a green route for precious & critical metal recovery and re-use, Green Chem. 17 (2015) 1951–1965.

[34] V.G. Zuin, V.L. Budarin, M. De bruyn, P.S. Shuttleworth, A.J. Hunt, C. Pluciennik, et al., Polysaccharide-derived mesoporous materials (Starbon®) for sustainable separation of complex mixtures, Faraday Discuss. 202 (2017) 451–464.

[35] H.L. Parker, J.R. Dodson, V.L. Budarin, J.H. Clark, A.J. Hunt, Direct synthesis of Pd nanoparticles on alginic acid and seaweed supports, Green Chem. 17 (2015) 2200–2207.

[36] J.C. Colmenares, P. Lisowski, D. Łomot, A novel biomass-based support (Starbon) for TiO2 hybrid photocatalysts: a versatile green tool for water purification, RSC Adv. 3 (2013) 20186–20192.

[37] S. Kim, A.M. Escamilla-Pérez, M. De Bruyn, J.G. Alauzun, N. Louvain, N. Brun, et al., Sustainable polysaccharide-derived mesoporous carbons (Starbon®) as additives in lithium-ion batteries negative electrodes, J. Mater Chem. A. 5 (2017) 24380–24387.

[38] H.R. Costantino, A.M. Feaver, William D. Scott, Manufacturing methods for the production of carbon materials, US8293818B2, 2012.

[39] R.J. Nemanich, S.A. Solin, First- and second-order Raman scattering from finite-size crystals of graphite, Phys. Rev. B. 20 (1979) 392–401.

[40] H.-Q. Li, R.-L. Liu, D.-Y. Zhao, Y.-Y. Xia, Electrochemical properties of an ordered mesoporous carbon prepared by direct tri-constituent co-assembly, Carbon. 45 (2007) 2628–2635.

[41] K.A. See, M.A. Lumley, G.D. Stucky, C.P. Grey, R. Seshadri, Reversible Capacity of Conductive Carbon Additives at Low Potentials: Caveats for Testing Alternative Anode Materials for Li-Ion Batteries, J. Electrochem. Soc. 164 (2016) A327–A333.

[42] Y. Wang, Y. Song, Y. Xia, Electrochemical capacitors: mechanism, materials, systems, characterization and applications, Chem. Soc. Rev. 45 (2016) 5925–5950.

[43] T. Brezesinski, J. Wang, S.H. Tolbert, B. Dunn, Ordered mesoporous alpha-MoO3 with iso-oriented nanocrystalline walls for thin-film pseudocapacitors, Nature Materials. 9 (2010) 146–151.

[44] A.J. Bard, L.R. Faulkner, Electrochemical Methods: Fundamentals and Applications, 2nd Edition, John Wiley & Sons, 2000.